

# Interstellar scintillations of PSR B1919+21: space-ground interferometry

V. I. Shishov,<sup>1\*</sup> T. V. Smirnova,<sup>1†</sup> C. R. Gwinn<sup>2‡</sup> A.S.Andrianov<sup>3§</sup>  
 M. V. Popov,<sup>3¶</sup> A. G. Rudnitskiy,<sup>3||</sup> V. A. Soglasnov<sup>3\*\*</sup>

<sup>1</sup>*Pushchino Radio Astronomy Observatory, Astro Space Center, Lebedev Physical Institute, Russian Academy of Sciences, Pushchino, Moscow oblast', 142290, Russia*

<sup>2</sup>*Department of Physics, University of California, Santa Barbara, California 93106, USA*

<sup>3</sup>*Astro Space Center, Lebedev Physical Institute, Russian Academy of Sciences, Profsoyuznaya 84/32, 117997, Russian Federation*

Accepted XXX. Received YYY; in original form 04.05.2016

## ABSTRACT

We carried out observations of pulsar PSR B1919+21 at 324 MHz to study the distribution of interstellar plasma in the direction of this pulsar. We used the RadioAstron (RA) space radiotelescope together with two ground telescopes: Westerbork (WB) and Green Bank (GB). The maximum baseline projection for the space-ground interferometer was about 60000 km. We show that interstellar scintillation of this pulsar consists of two components: diffractive scintillations from inhomogeneities in a layer of turbulent plasma at a distance  $z_1 = 440$  pc from the observer or homogeneously distributed scattering material to pulsar; and weak scintillations from a screen located near the observer at  $z_2 = 0.14 \pm 0.05$  pc. Furthermore, in the direction to the pulsar we detected a prism that deflects radiation, leading to a shift of observed source position. We show that the influence of the ionosphere can be ignored for the space-ground baseline. Analysis of the spatial coherence function for the space-ground baseline (RA-GB) yielded the scattering angle in the observer plane:  $\theta_{scat} = 0.7$  mas. An analysis of the time-frequency correlation function for weak scintillations yielded the angle of refraction in the direction to the pulsar:  $\theta_{ref,0} = 110$  ms and the distance to the prism  $z_{prism} \leq 2$  pc.

**Key words:** pulsars – scattering – ISM

## 1 INTRODUCTION

Fluctuations of electron density in the interstellar plasma scatter radiowaves from astronomical objects. The observer at the Earth detects a signal that is a convolution of the initial signal and a kernel that describes scattering in the interstellar plasma (Gwinn & Johnson 2011). Several effects are observed for pulsars corresponding to the scattering of the radio emission: intensity modulation in frequency and in time (scintillations), pulse broadening, angular broadening, and signal dispersion in frequency.

A space radiotelescope such as RadioAstron provides

a great opportunity to measure the parameters of scattering. Separation of the effects of close and distant scattering material requires high spatial resolution. RadioAstron provides the space element of this interferometer for our observations. Technical and measured parameters of the RadioAstron mission have been described by Avdeev et al. (2012) and Kardashev et al. (2013). We observed several close pulsars in the Early Science program of RadioAstron (RAES), including pulsars B0950+08 and B1919+21. First results, published in the paper of Smirnova et al. (2014) show that a layer of plasma located very close to the Earth, at 4.4 to 16.4 pc, is primarily responsible for scintillation of B0950+08. First indications that the nearest interstellar medium is responsible for the scintillations of pulsars B0950+08 and J0437-47 were discussed in earlier papers Smirnova & Shishov (2008); Smirnova et al. (2006); see also Bhat et al. (2016). These pulsars have among the lowest dispersion measures observed, indicating a low column density of plasma. A scattering medium located at a distance of about 10 pc from the Sun is also responsible for the variabil-

\* E-mail: shishov@prao.ru (PRAO ASC LPI)

† E-mail: tania@prao.ru (PRAO ASC LPI)

‡ E-mail: cgwinn@ucsb.edu (University of California)

§ E-mail: andrian@asc.rssi.ru (ASC LPI)

¶ E-mail: mwpopov@gmail.com (ASC LPI)

|| E-mail: almax1024@gmail.com (ASC LPI)

\*\* E-mail: vsoglasn@asc.rssi.ru (ASC LPI)

ity of some quasars over periods of about an hour, when observed at centimeter wavelengths (Kedziora-Chudczer et al. 1997; Dennett-Thorpe & deBruyn 2002; Bignall et al. 2003; Dennett-Thorpe & deBruyn 2003; Jauncey et al. 2003; Bignall et al. 2006). These observations of scattering of close pulsars and short-period variability of quasars indicate the existence of a nearby interstellar plasma component that has properties different from those of more distant plasma components.

The aim of the study reported here is to investigate the spatial distribution of the interstellar plasma toward the pulsar B1919+21. We show that two isolated layers of interstellar plasma lie in this direction, one of which is localized at a distance of only 0.14 pc. Pulsar B1919 + 21 is a strong pulsar. Its period is  $P_1 = 1.3373$  s. It lies at galactic latitude  $3.5^\circ$  and longitude  $55.8^\circ$ . Its dispersion measure is  $DM = 12.43$  pc cm $^{-3}$ . The Cordes & Lazio (2003) model indicates that the pulsar distance is 1 kpc. Measurements of this pulsar's proper motion yielded  $\mu_\alpha = 17 \pm 4$  mas/yr and  $\mu_\delta = 32 \pm 6$  mas/yr (Zou et al. 2005).

## 2 OBSERVATIONS

We conducted observations of PSR B1919+21 at an observing frequency of 324 MHz on 4 July 2012, using the RadioAstron 10-m space radiotelescope together with 110-m Green Bank (GBT) and 14×25-m Westerbork (WSRT) telescopes. Data were transferred from RadioAstron in real time to Puschino, where they were recorded using the RadioAstron Digital Recorder (RDR) (Andrianov et al. 2014), developed at the Astro-Space Center of the Lebedev Physical Institute (ASC). The Mark5B recording system was used for the ground telescopes. All telescopes recorded the frequency band from 316 to 332 MHz, with one-bit quantization for space telescope data, and two-bit quantization for ground telescopes. Data were recorded for 4170 s, divided into scans of  $421 P_1$  (563 s) and subintervals of  $26 P_1$  (about 35 s). The primary data processing was done using the ASC correlator (Andrianov et al. 2014) with incoherent dedispersion. Data were correlated with 512 spectral channels in two selected windows: on pulse and off pulse, the width of each window was 40 ms (3% of the pulsar period). An on-pulse window was centered on the maximum of the average profile, and an off-pulse window was selected at half the pulsar period from the on-pulse window. The projected space-ground interferometer baseline was about 60,000 km.

## 3 DATA PROCESSING AND ANALYSIS

### 3.1 Dynamic Spectrum and Correlation Functions

#### 3.1.1 Dynamic Spectrum

We formed complex cross-spectra between pairs of telescopes for all scans, in on- and off-pulse windows. In some cases, to increase the sensitivity, we averaged cross-spectra over 4 pulsar periods. To obtain dynamic spectra, we calculated the modulus of the cross-spectra, and corrected for the receiver bandpass using the off-pulse spectra. To reduce the impact of broadband intensity variations of the pulsar from

pulse to pulse, we normalized each spectrum by its standard deviation,  $\sigma(t)$ . Figure 1 shows the normalized dynamic spectrum of scintillation of pulsar B1919+21 for the Green Bank - Westerbork ground interferometer (GB-WB). We see clearly expressed large-scale sloping structures (slanting features), with scales of  $df = 1$  to 1.5 MHz in frequency, and of  $dt \approx 1000$  s in time. Diffractive spots are strongly extended along the line  $f = (df/dt)t$ . This drift indicates that refraction by a cosmic prism determines the structure of scintillation in the frequency-time domain. The regular dark bands along the frequency axis represent the intervals when signal was not recorded, and were filled with values of zero. The narrower gray bands show the pulse-to-pulse variability intrinsic to the pulsar.

#### 3.1.2 Drift and Dual Frequency Scales

To determine the drift rate of the diffractive structure, we calculated the position of maximum of the mean cross-correlation between spectra separated in time by lags  $kP_1$ , where  $k = 1, 2, \dots$  and  $P_1$  is a pulse period in s. We found three separated bands with the slope  $\Delta f/\Delta t = 1.5$  MHz/1000s. We obtained this slope by a least-squares fit to the positions of maximums. Figure 2 shows spectra of several strong pulses separated in time, with time increasing from bottom to top in the figure.

Two scales of structure are visible in the spectra: small-scale structure with a frequency scale of about 400 kHz, and large-scale structure with frequency scale of about 1500 kHz. These scales are the approximate full width at half-maximum amplitude of the features. At smaller separations in time (as in spectra a and b in the figure, separated by 11 s), the fine structure is the same. Over longer separations (as in spectra b and c, separated by 200 s) the fine structure changes, but the large-scale structure retains its shape. The modulation index, defined as  $m(t) = \sigma(t)/(I)_f(t)$ , varies from 0.7 to 1.0 on a time scale of the order of 500 s. This variation indicates that the statistics are not sufficient to determine the correct value of  $m(t)$ . However, the fact that the modulation index is close to 1 confirms that the scattering is strong.

#### 3.1.3 Determination of Frequency Scales

A correlation analysis of the dynamic spectra provides the scales of scintillation in frequency,  $\Delta f_{dif}$ . Figure 3 shows the average autocorrelation functions (ACF) as a function of frequency lag. The ACF was averaged over the entire observation. For our ground baseline we calculated the ACF using the usual procedure, because the influence of noise was small, and because it was necessary to eliminate the influence of the ionosphere, as discussed below. For the space-ground baseline, we calculated the ACF as the modulus of the average correlation function of the complex cross-spectra. The corresponding expressions are presented in the Section 3.2. This procedure is required when the contribution of the noise is greater than or comparable to the signal level, and when ionospheric effects are small, as was the case for our space-ground baseline. Otherwise, the contribution of noise will distort the ACF.

The visible break in the slope of the ACF near a lag

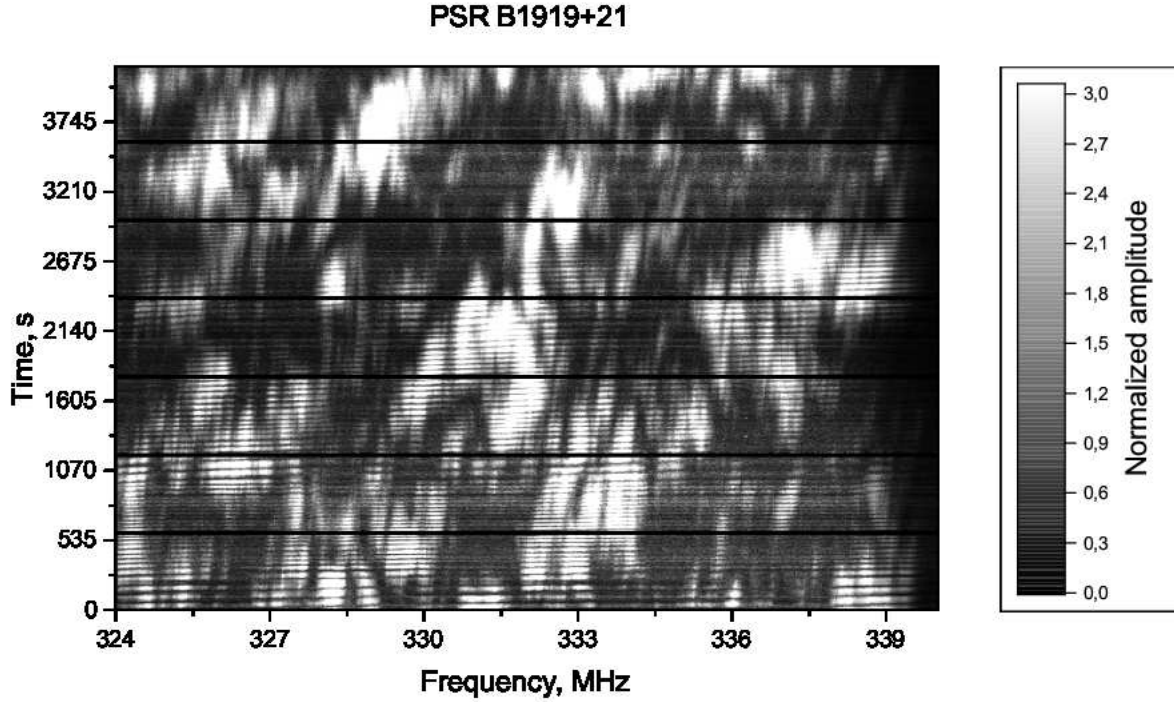


**Figure 1.** Dynamic spectrum of PSR B1919+21 at observing frequency 324 MHz, for the ground baseline Green Bank - Westerbork (GB-WB). Grayscale shows normalized amplitude.

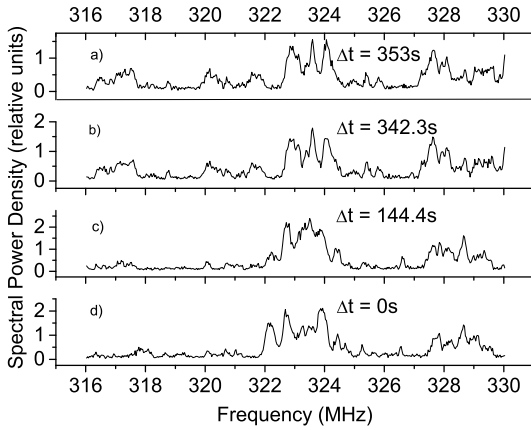


**Figure 2.** Spectra of individual pulses of the pulsar, separated in time by the specified number of seconds from the bottom spectrum.

of  $\pm 300$  kHz for the ground baseline (GB-WB: Figure 3, lower), indicates the presence of structure on two scales. No break appears in the ACF for the space-Earth baseline: its shape corresponds to the small-scale structure only. To determine the widths and the relative amplitudes of these structures we fit the ground baseline with a sum of exponential and Gaussian functions. We obtained frequency scales of  $\Delta f_{dif} = 330$  kHz and  $\Delta f_{wide} = 700$  kHz (half width at half-maximum amplitude), with amplitudes of 0.84 and 0.15 for the small- and large-scale structures, respectively. As it

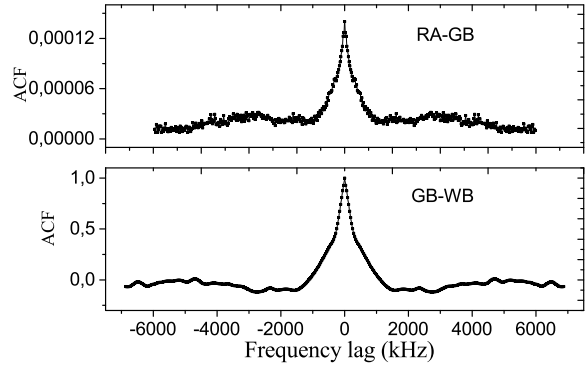


**Figure 3.** Autocorrelation functions (ACF) averaged over the entire observation time for space-ground (RA-GB, upper) and ground (GB-WB, lower) baselines. Expression 10 was used to calculate the ACF for the space-ground baseline.

will be shown below in Section 4, the small-scale structures arise from scattering of radiation in the distant layer of the turbulent medium as diffractive scintillation, and the large-scale structures in the layer located close to observer as weak scintillation.

#### 3.1.4 Determination of Time Scale

Figure 4 shows the average cross-correlation coefficient between pairs of spectra as a function of time for space-ground

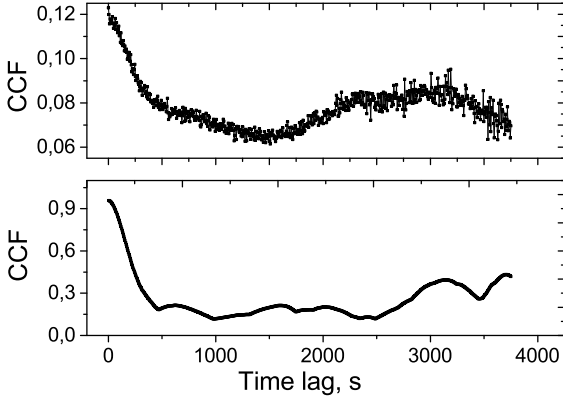


**Figure 4.** The dependence of the average cross-correlation coefficient between pairs of spectra spaced by the corresponding time interval  $\Delta t = 4P_1k$ ,  $k = 1, 2, \dots$ , for space-ground (upper) and ground (lower) baselines.

(upper) and ground (lower) baselines. The time separations are  $\Delta t = 4P_1k$ , where  $k = 1, 2, \dots$ . Both baselines show the same scintillation scale:  $\Delta t_{dif} = 290$  s, expressed as the time lag of  $1/e$  of the peak amplitude.

### 3.2 Theoretical relations, ionospheric effects, correlation functions

Much of our analysis in this paper follows that of [Smirnova et al. \(2014\)](#) in general outline, but here we describe new details connected with ionospheric effects and use different definitions for the correlation functions. Let  $h(f, t)$  be the spectrum of the field of initial pulsar emission in the absence of any turbulent medium, where  $f = \nu - \nu_0$  is the offset of the observing frequency  $\nu$  from the band center  $\nu_0 = 324$  MHz, and  $t$  is time. This spectrum  $h(f, t)$  also includes instrumental modulation of emission in the passbands of the receivers. After propagation through the turbulent interstellar medium, the spectrum of the electric field for one antenna can be represented as:

$$E(\vec{\rho}, f, t) = h(f, t)u(\vec{\rho}, f, t) \exp[-iS(\vec{\rho}, f, t)], \quad (1)$$

where the modulation coefficient  $u(\vec{\rho}, f, t)$  is determined by propagation through the interstellar medium, and  $\vec{\rho}$  is the spatial coordinate in the observer plane, perpendicular to the line of sight. The phase  $S(\vec{\rho}, f, t)$  is determined by the ionosphere and cosmic prism. Multiplying  $E(\vec{\rho}, f, t)$  by  $E^*(\vec{\rho} + \vec{b}, f, t)$  and averaging over the statistics of the source, we obtain the quasi-instantaneous response of an interferometer with a baseline  $\vec{b}$ , the cross-spectrum of the electric field:

$$\begin{aligned} I(\vec{\rho}, \vec{\rho} + \vec{b}, f, t) &= E(\vec{\rho}, f, t)E^*(\vec{\rho} + \vec{b}, f, t) \\ &= H(f, t)j(\vec{\rho}, \vec{\rho} + \vec{b}, f, t) \\ &\quad \times \exp[-i\Delta S(\vec{\rho}, \vec{b}, f, t)] \end{aligned} \quad (2)$$

where:

$$j(\vec{\rho}, \vec{\rho} + \vec{b}, f, t) = u(\vec{\rho}, f, t)u^*(\vec{\rho} + \vec{b}, f, t) \quad (3)$$

$$H(f, t) = \langle h(f, t)h^*(f, t) \rangle_h \quad (4)$$

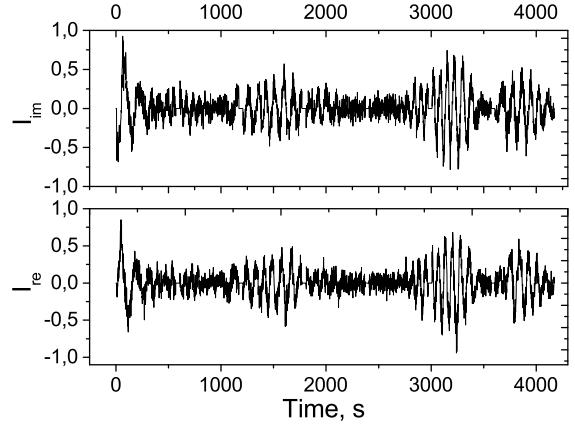


**Figure 5.** Dependencies of the real (upper) and imaginary (lower) parts of the complex cross-spectrum on time for frequency channel 100, for the Green Bank-Westerbork baseline (GB-WB). Data were not recorded during intervals indicated as zero amplitude.

The subscript  $h$  indicates averaging over the statistics of the noiselike electric field of the source. We assume that the intrinsic spectrum of the source, and of our instrumental response, is flat:  $H(f, t) = 1$ . The phase difference between the antennas at either end of the baseline  $\Delta S(\vec{\rho}, f, t)$  consists of two components, from interstellar refraction and from the ionosphere:

$$\Delta S(\vec{\rho}, \vec{b}, f, t) = \Delta S_{ion}(\vec{\rho}, \vec{b}, f, t) + \Delta S_{ref}(\vec{b}, f) \quad (5)$$

For a fixed baseline, the refractive component of the interferometer phase,  $\Delta S_{ref}(\vec{b}, f)$  depends only on  $f$ :

$$\Delta S_{ref}(\vec{b}, f) = 2\pi \left( \frac{f}{c} \right) \vec{b} \cdot \vec{\Theta}_{ref,0} \quad (6)$$

Here  $\vec{\Theta}_{ref,0}$  is the refraction angle at frequency  $\nu_0$ .

The ionospheric component can be represented as

$$\begin{aligned} \Delta S_{ion}(\vec{\rho}, \vec{b}, f, t) &= \Delta S_{ion}(\rho, \vec{b}, f = 0, t) + \frac{f}{\nu_0} \Delta S_{ion,0} \\ &\quad + \frac{f}{\nu_0} \frac{(t - t_0)}{T} \Delta S_{ion,1} \end{aligned} \quad (7)$$

$$\Delta S_{ion,0} = \Delta S_{ion}(\vec{\rho}, \vec{b}, f = 0, t = t_0)$$

$$\Delta S_{ion,1} = T \frac{d}{dt} [\Delta S_{ion}(\vec{\rho}, \vec{b}, f = 0, t)] |_{t=t_0}$$

where  $T$  is the time span of the observations, and  $t_0$  is the time at the middle.

Figure 5 shows the values of the real and imaginary parts of the interferometer response for one selected frequency channel as a function of time:  $\text{Re}[I(\rho, \rho + b, f, t)]$  (upper) and  $\text{Im}[I(\rho, \rho + b, f, t)]$  (lower). In addition to the amplitude fluctuations corresponding to the dynamic spectrum, we see periodic fluctuations with a characteristic period of about 70 s, phase-shifted by  $90^\circ$ . Changes of the ionosphere in time cause these fluctuations. Therefore, to analyze the data from the ground interferometer we must work with the moduli of the cross-spectra. For the space-ground interferometer, the influence of ionosphere was much smaller, as will be shown below, and so data processing used the complex cross-spectra.

Multiplying  $I(\vec{\rho}, \vec{\rho} + \vec{b}, f, t)$  by its complex conjugate at

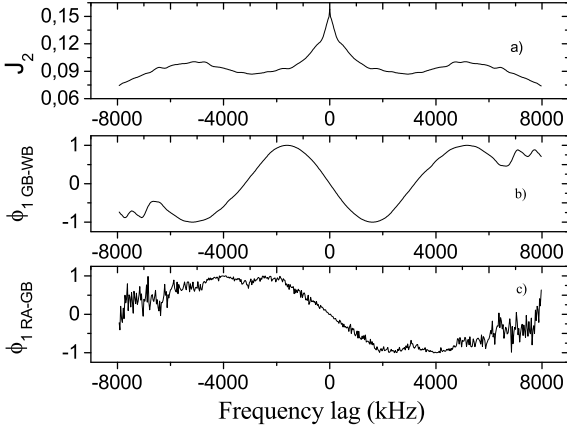


**Figure 6.** a) Average modulus of the correlation of  $I$  with frequency offset  $f$  (Equation 11); b)  $\varphi_1(f)$ , the ratio of the imaginary part of the correlation to its modulus for the ground interferometer (GB-WB) as a function of  $f$ ; c) the same ratio  $\varphi_1(f)$  for the space-ground interferometer (RA-GB).

frequency  $f + \Delta f$  (where  $\Delta f =$  frequency shift) and averaging over time and frequency, we obtain

$$\begin{aligned} & \langle I(\vec{\rho}, \vec{\rho} + \vec{b}, f, t) I^*(\vec{\rho}, \vec{\rho} + \vec{b}, f + \Delta f, t) \rangle \\ &= \langle j(\vec{\rho}, \vec{\rho} + \vec{b}, f, t) j^*(\vec{\rho}, \vec{\rho} + \vec{b}, f + \Delta f, t) \rangle \varphi(\Delta f) \\ & \times \exp[-i(\Delta f/\nu_0)[\Delta S_{ion,0} + \Delta S_{ref,0}]] \end{aligned} \quad (8)$$

where:

$$\begin{aligned} \varphi(\Delta f) &= \left\langle \exp \left[ -i \left( \frac{\Delta f}{\nu_0} \right) \frac{(t - t_0)}{T} \Delta S_{ion,1} \right] \right\rangle_t \\ &= \frac{\sin[(\Delta f/2\nu_0)\Delta S_{ion,1}]}{(\Delta f/2\nu_0)\Delta S_{ion,1}} \end{aligned} \quad (9)$$

In Equation 9, the average corresponds to an integration over  $t$  from  $(t_0 - T/2)$  to  $(t_0 + T/2)$ . The phase difference at frequency  $\nu_0$  is  $\Delta S_{ref,0}$ .

The modulus of the averaged correlation in frequency  $f$  of the interferometer response  $I$  is:

$$J_1(\vec{b}, \Delta f) = |\langle I(\vec{\rho}, \vec{\rho} + \vec{b}, f, t) I^*(\vec{\rho}, \vec{\rho} + \vec{b}, f + \Delta f, t) \rangle| \quad (10)$$

In contrast, the averaged modulus of the correlation in frequency of  $I$  is:

$$\begin{aligned} J_2(\vec{b}, \Delta f) &= \langle |I(\vec{\rho}, \vec{\rho} + \vec{b}, f, t) I^*(\vec{\rho}, \vec{\rho} + \vec{b}, f + \Delta f, t)| \rangle \\ &= \langle j(\vec{\rho}, \vec{\rho} + \vec{b}, f, t) j^*(\vec{\rho}, \vec{\rho} + \vec{b}, f + \Delta f, t) \rangle \end{aligned} \quad (11)$$

Figure 3 (upper panel) shows the modulus of the averaged correlation function of  $I$  for the space-ground interferometer, as defined in Equation 10. The imaginary part of the second moment divided by its modulus is  $\varphi_1(\Delta f)$ . The function  $\varphi_1(\Delta f)$  is proportional to  $\varphi(\Delta f) * \sin[-\Delta f/\nu_0(\Delta S_{ion,0} + \Delta S_{ref,0})]$ .

Figure 6 shows values of  $J_2(\Delta f)$  and  $\varphi_1(\Delta f)$  for the ground interferometer, and  $\varphi_1(\Delta f)$  for the space-ground interferometer. We see that for the ground interferometer the ionospheric phase is larger and varies more rapidly with frequency than for the space-ground interferometer.

The value of  $\varphi_1(\Delta f)$  is zero at  $\Delta f = 0$ , as defined by the factor  $\sin[-\Delta f/\nu_0(\Delta S_{ion,0} + \Delta S_{ref,0})]$ . However, the zeros of  $\varphi_1(\Delta f)$  for the ground interferometer at  $\Delta f = \pm 3$  MHz are defined by  $\varphi(\Delta f)$ . If we set the argument of  $\varphi$  in Equation 9

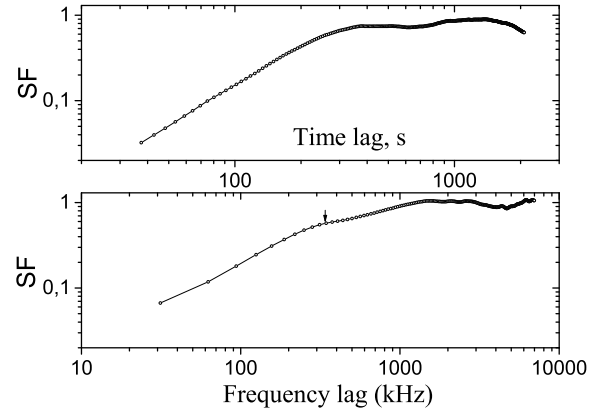


**Figure 7.** Average time (upper) and frequency (lower) structure functions of intensity variations (SF) for Green Bank - Westerbork (GB-WB) baseline, presented on a log-log scale. The arrow marks the frequency lag of the observed break in the structure function, 300 kHz.

equal to  $\pi$  at  $\Delta f = 3$  MHz, we obtain  $\Delta S_{ion,1} \approx 600$  radians for the ground interferometer, and  $\Delta S_{ion,1} \leq 200$  radians for the space-ground interferometer. From these values, it follows that the response of the ground interferometer is greatly distorted by the ionospheric phase, but the signal amplitude greatly exceeds the noise. Thus, we use Equation 11 to calculate the correlation function of amplitude fluctuations for the ground baseline. For the space-ground interferometer, the situation is reversed: noise exceeds the signal, and we cannot use Equation 11. However, we can neglect the phase distortion of the interferometer response, and use Equation 10 to determine correlation functions of amplitude fluctuations on the space-ground baseline.

### 3.3 Structure functions of the interferometer response fluctuations

Structure functions provide insight into the correlation function, as discussed in earlier papers (Smirnova et al. 2014). For the space-ground interferometer on baseline  $\vec{b}_s$  we calculate the structure function in frequency difference  $\Delta f$  and time difference  $\Delta t$  using  $J_1(\vec{b}_s, \Delta f = 0, \Delta t = 0) - J_1(\vec{b}_s, \Delta f, \Delta t)$ . We normalize this expression by  $J_1(\vec{b}_s, \Delta f = 0, \Delta t = 0) - J_1(\vec{b}_s, \Delta f^*, \Delta t = 0)$ , where  $\Delta f^* \gg \Delta f_{dif}$ . Hence we obtain the structure function for the space-ground interferometer:

$$\begin{aligned} SF_s(\vec{b}_s, \Delta f, \Delta t) & \\ &= \frac{\left( J_1(\vec{b}_s, \Delta f = 0, \Delta t = 0) - J_1(\vec{b}_s, \Delta f, \Delta t) \right)}{\left( J_1(\vec{b}_s, \Delta f = 0, \Delta t = 0) - J_1(\vec{b}_s, \Delta f^*, \Delta t = 0) \right)} \end{aligned} \quad (12)$$

Similarly, the structure function for the ground interferometer with baseline  $\vec{b}_g$  yields the normalized structure function

$$\begin{aligned} SF_g(\vec{b}_g, \Delta f, \Delta t) & \\ &= \frac{\left( J_2(\vec{b}_g, \Delta f = 0, \Delta t = 0) - J_2(\vec{b}_g, \Delta f, \Delta t) \right)}{\left( J_2(\vec{b}_g, \Delta f = 0, \Delta t = 0) - J_2(\vec{b}_g, \Delta f^*, \Delta t = 0) \right)} \end{aligned} \quad (13)$$

Figure 7 shows average time (upper) and frequency

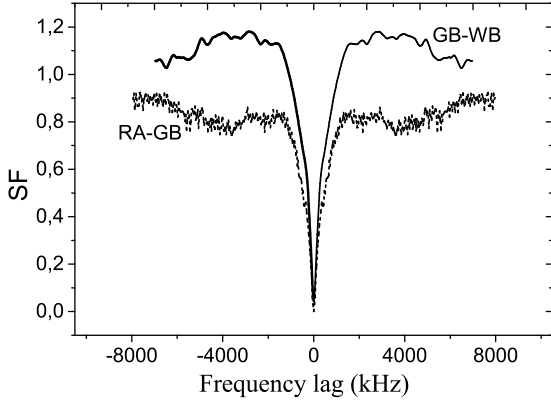


**Figure 8.** Normalized frequency structure functions of intensity variations for ground (GB-WB) and space-ground (RA-GB) baselines at zero time shift.

(lower) structure functions (SF) of intensity variations for our ground baseline on log-log axes.

An arrow marks the break in the structure function at a frequency lag of 300 kHz. We fit power-laws to the structure functions:

$$SF(\Delta f) = \frac{1}{2} (\Delta f / \Delta f_{dif})^{\beta_f} \quad (14)$$

$$SF(\Delta t) = \frac{1}{2} (\Delta t / \Delta t_{dif})^{\beta_t}$$

We performed linear fits to the logarithmic data for these two structure functions over the ranges  $\Delta t_{samp} < \Delta t < \Delta t_{dif}$  and  $\Delta f_{samp} < \Delta f < \Delta f_{dif}$  respectively, where  $\Delta t_{samp}$  and  $\Delta f_{samp}$  are the sampling intervals in time and frequency for our data. We obtained  $\beta_f = 0.90 \pm 0.03$  for the frequency structure function and  $\beta_t = 1.73 \pm 0.02$  for the time structure function. The resulting relation between frequency and time structure functions  $\beta_f = \beta_t/2$  corresponds to a diffractive model for scintillation (Shishov et al. 2003). The power-law index  $n$  of the spectrum of density inhomogeneities responsible for scattering is connected with the index of  $SF(t)$  through the relation:  $n = \beta_t + 2 = 3.73$  (Shishov et al. 2003).

Figure 8 shows the average frequency structure functions for the ground (line) and space-ground (dash line) baselines at zero time shift. Evidently the levels of the SF differ by about 0.2 - 0.3. This corresponds to the relative contributions of the two frequency scales in the scintillation spectra to the ground baseline, as seen in Figures 2 and 3, and discussed in Section 3.1.3 above. The ratio of their amplitudes is consistent with our fit to two components in the average frequency correlation function for the ground baseline. The space-ground baseline shows no such break in the structure function in Figure 8, or what would be corresponding structure in the correlation function shown in Figure 3. Rather, the space-ground structure function displays only the narrower frequency-scale component.

Figure 9 shows the mean frequency structure functions for the ground baseline at different time lags:  $4P_1$  (squares),  $200P_1$  (circles),  $320P_1$  (line) and  $640P_1$  (triangles). With increasing time shift between spectra, the amplitude of the structure function decreases, and its minimum is displaced. When  $\Delta t = 200P_1$  (267 s) the structure function still shows

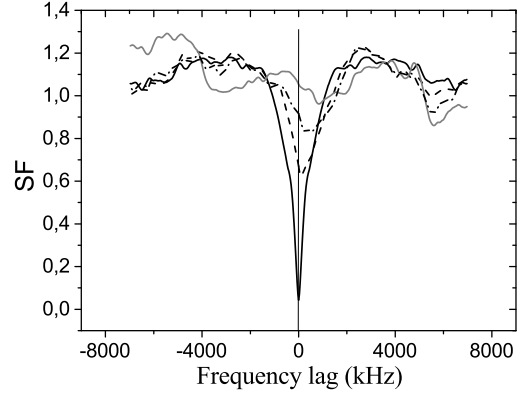


**Figure 9.** Average structure functions of intensity variations for Green Bank - Westerbork baseline, calculated from spectra for different time shifts: black line for  $\Delta t = 4P_1$ ; dash line for  $\Delta t = 200P_1$ ; dash-dot line for  $\Delta t = 320P_1$ ; grey line for  $\Delta t = 640P_1$

a small contribution of small-scale structure, whereas at  $\Delta t = 640P_1$  (856 s) we see only one component, the center of which is shifted to 1100 kHz, with amplitude of 0.15. Weak scintillation alone would produce a wide-bandwidth pattern; but the cosmic prism slants the pattern in both frequency, by dispersion; and in time, by a spatial displacement that the motion of the source converts to the time domain. Thus, a frequency shift compensates for the time offset, as Figure 9 displays. This effect is also clearly visible in the dynamic spectrum (Figure 1) as was discussed in Section 3.1.2. The drift in frequency at the rate  $df/dt = 1.1$  MHz over 856 s = 1.3 MHz/1000 s is close to that obtained in Section 3.1.2 above,  $df/dt = 1.5$  MHz/1000 s. We will adopt the rate of 1.5 MHz/1000 s as more accurate because the structure function for large time shift is weak and has a large variations.

For the space-ground baseline (RA-GB), a time shift of the structure function produces only a decrease in the amplitude of the structure function, without displacement of its minimum, even with time shifts as large as 800 s. This is consistent with absence of the wide structure on the long baseline. We further conclude that the refraction that causes displacement of the structure function takes place behind the screen responsible for diffractive scintillation.

### 3.4 Spatial coherence function

According to Equation 10,  $J_1(\vec{b}, \Delta f)$  is the second moment of  $j(\vec{\rho}, \vec{\rho} + \vec{b}, f, t)$  and also is the fourth moment of the field  $u(\vec{\rho}, f, t)$ . As Prokhorov et al. (1975) showed, the fourth moment of the field can be expressed through the second moments and, in the regime of strong scintillations

$$J_1(\vec{b}, \Delta f) = |\langle j(\vec{\rho}, \vec{\rho} + \vec{b}, f, t) j^*(\vec{\rho}, \vec{\rho} + \vec{b}, f + \Delta f, t) \rangle|$$

$$= |B_u(f)|^2 + |B_u(\vec{b})|^2. \quad (15)$$

Here  $B_u(\vec{b})$  is the spatial field-coherence function at a single average flux, and  $B_u(f)$  is the frequency correlation function of fluctuations in flux, and is independent of baseline. If the spatial coordinate in the phase screen plane is  $\Delta \vec{\rho}$  then

(Prokhorov et al. 1975):

$$B_u(\Delta\vec{\rho}) = \exp[-\frac{1}{2}D_s(\Delta\vec{\rho})], \quad (16)$$

where  $D_s(\Delta\vec{\rho})$  is the spatial structure function of phase fluctuations:

$$D_s(\Delta\vec{\rho}) = \langle \phi(\vec{x} + \Delta\vec{\rho}) - \phi(\vec{x}) \rangle_{\vec{x}} \quad (17)$$

where  $\phi(\vec{x})$  is the screen phase at  $\vec{x}$ . In the case of a spherical wave at the observer plane we have

$$D_s(\Delta\vec{\rho}) = \int_0^z dz' D(\Delta\vec{\rho}) \quad (18)$$

where  $D$  is a gradient of  $D_s(\Delta\vec{\rho})$  along the  $z$ -axis and  $\Delta\vec{\rho} = \frac{(z-z')}{z}\vec{b}$ . The integration is from the observer at  $z' = 0$  to the pulsar at  $z' = z$ .

For the space-ground interferometer we used Equation 15 with  $b = b_s$ , where  $b_s$  is the interferometer baseline. According to Equation 15, for  $\Delta f = 0$  we have  $J_1(\vec{b}_s, \Delta f = 0) = 1 + |B_u(\vec{b}_s)|^2$ ; and for  $\Delta f > \Delta f_{dif}$  we have  $J_1(\vec{b}_s, \Delta f > \Delta f_{dif}) = |B_u(\vec{b}_s)|^2$ . As displayed in Figure 3, we find  $J_1(\vec{b}_s, \Delta f = 0) = 1.4 \times 10^{-4}$  and  $J_1(\vec{b}_s, \Delta f > \Delta f_{dif}) = 2.4 \cdot 10^{-5}$  at  $\Delta f = 2$  MHz. Thus,

$$\frac{J_1(\vec{b}_s, \Delta f > \Delta f_{dif})}{J_1(\vec{b}_s, \Delta f = 0)} = \frac{|B_u(\vec{b}_s)|^2}{1 + |B_u(\vec{b}_s)|^2} = 0.17 \quad (19)$$

From this equation, we obtain

$$|B_u(\vec{b}_s)|^2 = 0.20 \quad (20)$$

From the analogous calculation for the ground interferometer (Figure 6a) we obtain

$$\frac{J_2(\vec{b}_g, \Delta f > \Delta f_{dif})}{J_2(\vec{b}_g, \Delta f = 0)} = \frac{|B_u(\vec{b}_g)|^2}{[1 + |B_u(\vec{b}_g)|^2]} = 0.50 \quad (21)$$

This implies

$$|B_u(\vec{b}_g)|^2 = 1. \quad (22)$$

This result implies that the ground interferometer does not resolve the scattering disk; mathematically, it means that  $|b_g| \ll 1/k\theta_{scat}$ .

#### 4 MODEL OF THE TURBULENT INTERSTELLAR MEDIUM

Our analysis leads to the following model for the scintillation. The material responsible for scintillation of PSR B1919+21 consists of two components: strong diffractive scattering in a layer of turbulent density inhomogeneities at a distance of  $z_1$ , that is responsible for the small-scale structure in the spectra; and weak and refractive scattering in a layer of turbulent density inhomogeneities close to the observer, at a distance of  $z_2$ , that is responsible for the large-scale structure. The spatial structure function of phase fluctuations  $D_s(\Delta\rho)$ , as described in Section 3.4 above, characterizes the two screens.

We describe here a physical model for the distribution of scattering material that explains our observations. Suppose we have a cosmic prism, located close to the observer at a

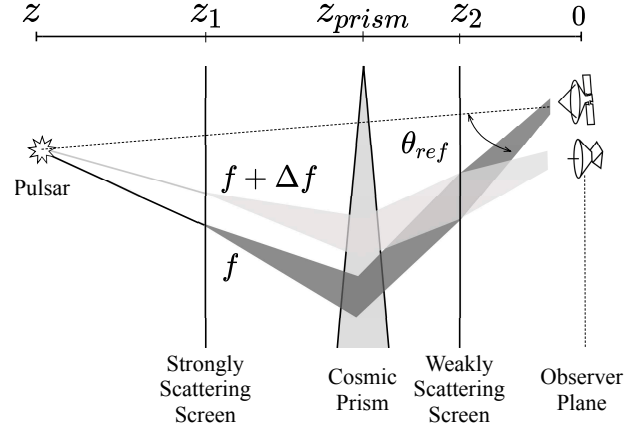


**Figure 10.** Schematic illustration of model geometry, showing radiation at a lower frequency  $f$  (dark line) scattered by the strongly-scattered screen 1 into a range of angles (dark shading), deflected by the cosmic prism, and further scattered by the weakly-scattering screen 2 before reaching the observer plane. Lighter path and shading shows a higher frequency  $f + \Delta f$ .

distance of  $z_{prism}$ , which deflects the beam with an angle of refraction  $\Delta\theta_{ref}$ . Let  $\vec{\theta}_{ref,0}$  be the resulting shift of source position visible in the observer plane at frequency  $\nu_0$ . The difference in refraction angle at a nearby frequency  $\nu_0 + f$  is Shishov et al. (2003)

$$\Delta\vec{\theta}_{ref} = 2\frac{f}{\nu_0}\vec{\theta}_{ref,0} \quad (23)$$

Suppose further that phase screen 2 is located close to the observer and the distance between the observer and the phase screen 2 is much smaller than  $z$ , the distance between the observer and the pulsar:

$$z_2 \ll z \quad (24)$$

The cosmic prism also located close to the observer, but a little bit further than the phase screen 2

$$z_2 < z_{prism} \ll z \quad (25)$$

Phase screen 1 is located much further away along the line of sight, at a distance of order  $z/2$ . The structure functions of phase fluctuations for the phase screens then have the model forms (Smirnova et al. 1998):

$$D_{S,1}(\Delta\vec{\rho}) = (k\theta_{scat,1}|\Delta\vec{\rho}|)^{\alpha_1}, \quad (26)$$

$$D_{S,2}(\Delta\vec{\rho}) = (k\theta_{scat,2}|\Delta\vec{\rho}|)^{\alpha_2}, \quad (27)$$

Thus, our model for the turbulent plasma towards the pulsar is characterized by the following parameters:  $\vec{\theta}_{ref,0}, \theta_{scat,1}, \theta_{scat,2}, \alpha_1, \alpha_2, z_1, z_2, z_{prism}$ . Figure 10 illustrates the geometry.

This model has similar structure to that used for our studies of the scintillations of pulsar B0950+08 Smirnova et al. (2014). However, in the present case the distance to phase screen 1 is considerably greater, and the characteristic scattering angle  $\theta_{scat,1}$  is significantly larger. Thus, for pulsar B1919+21 the scintillations are strong and saturated, with modulation index close to 1, as discussed in Section 3.1.2. Accordingly, we apply the theory of saturated

scintillations [Prokhorov et al. \(1975\)](#). In this case, the field coherence function  $B_u(\vec{b})$  is given by:

$$\begin{aligned} \langle j(\vec{\rho}, \vec{\rho} + \vec{b}, f, t) \rangle &= \langle u(\vec{\rho}, f, t) u^*(\vec{\rho} + \vec{b}, f, t) \rangle \\ &= B_u(\vec{b}) \\ &= \exp \left[ -\frac{1}{2} D_{S,1} \left( \frac{(z-z_1)}{z} \vec{b} \right) - \frac{1}{2} D_{S,2}(\vec{b}) \right] \end{aligned} \quad (28)$$

For the distant screen 1, the sphericity of the wavefront at the screen is important, and the conversion of the baseline in the observer's plane  $\vec{b}$  to the distance between the beams in the phase screen plane is given by the equation:

$$\Delta \vec{\rho}_{1,b} = \frac{(z-z_1)}{z} \vec{b} \quad (29)$$

For the closer phase screen 2 we can neglect the sphericity factor.

For saturated scintillations, the second moment  $j(\vec{\rho}, \vec{\rho} + \vec{b}, f, t)$  consists of two components: diffractive and refractive ([Prokhorov et al. 1975](#)). The diffractive component can be represented as

$$\begin{aligned} J(\vec{b}, \Delta f, \Delta t)_{dif} &= \langle j(\vec{\rho}, \vec{\rho} + \vec{b}, f, t) \\ &\quad \times j^*(\vec{\rho}, \vec{\rho} + \vec{b}, f + \Delta f, t + \Delta t) \rangle_{dif} \\ &= \langle j(\vec{\rho}, \vec{\rho} + \vec{b}, f, t) \rangle \langle j^*(\vec{\rho}, \vec{\rho} + \vec{b}, f, t) \rangle \\ &\quad + B_j(\Delta f, \Delta t) \end{aligned} \quad (30)$$

Here  $B_j(\Delta f, \Delta t)$  is a frequency-time correlation function of flux fluctuations independent of the projected baseline:

$$\begin{aligned} B_j(\Delta f, \Delta t) &= \langle u(\vec{\rho}, f, t) u^*(\vec{\rho}, f + \Delta f, t + \Delta t) \rangle \\ &\quad \times \langle u(\vec{\rho} + \vec{b}, f, t) u^*(\vec{\rho} + \vec{b}, f + \Delta f, t + \Delta t) \rangle \\ &= |B_u(\Delta f, \Delta t)|^2 \end{aligned} \quad (31)$$

Pulsar motion at a transverse speed of  $\vec{V}_p$  is primarily responsible for variations of flux density with time, producing scintillations from phase screen 1 at distance  $z_1$ . Pulsar motion leads to a shift of the beam in the plane of the phase screen:

$$\Delta \vec{\rho}_{1,t} = \frac{z_1}{z} \vec{V}_p \Delta t \quad (32)$$

For  $\Delta f = 0$  we have

$$\begin{aligned} B_u(\Delta t) &= \exp \left[ -\frac{1}{2} D_{S,1}(\Delta \vec{\rho}_{1,t}) \right] \\ &= \exp \left[ -\frac{1}{2} \left( \frac{\Delta t}{\Delta t_{dif}} \right)^{\alpha_1} \right] \end{aligned} \quad (33)$$

with

$$\Delta t_{dif} = \frac{z}{z_1 k \theta_{scat,1} |\vec{V}_p|} \quad (34)$$

Correspondingly,

$$B_j(\Delta t) = \exp[-D_{S,1}(\Delta \vec{\rho}_{1,t})] = \exp[-(\Delta t / \Delta t_{dif})^{\alpha_1}] \quad (35)$$

For a ground baseline, the projected length  $b_g$  is much smaller than the coherence scale of the field  $1/k\theta_{scat,1}$ :

$$b_g \ll \frac{1}{k\theta_{scat,1}} \quad (36)$$

and correspondingly,

$$B_u(\vec{\rho}, \vec{\rho} + \vec{b}_g) = 1. \quad (37)$$

For a space-ground baseline, the projected length  $b_s$  is larger than the coherence scale of the field:

$$b_s > \frac{1}{k\theta_{scat,1}} \quad (38)$$

and correspondingly,

$$B_u(\vec{\rho}, \vec{\rho} + \vec{b}_s) = \exp \left[ -\frac{1}{2} \left( \frac{z-z_1}{z} \cdot \frac{b_s}{k\theta_{scat,1}} \right)^{\alpha_1} \right] \quad (39)$$

Here,  $[(z-z_1)/z]$  is the sphericity factor, which converts the baseline  $b_s$  into the distance between beams in the phase screen plane at distance  $z_1$ . Comparison of  $J(\vec{b}, \Delta f = 0)$  and  $J(\vec{b}, \Delta f > \Delta f_{dif})$  allows us to estimate the spatial coherence function (interferometer visibility), as in Section 3.4 above.

## 5 RESULTS

As mentioned above, the time correlation function of interferometer response fluctuations is determined primarily by pulsar motion with transverse velocity  $\vec{V}_p$ . Pulsar motion shifts the beam in the plane of phase screen 1 by  $\Delta \vec{\rho}_{1,t}$  (Equation 32). The temporal correlation function of flux density shown in Figure 4 yields  $\Delta t_{dif} = 290$  s. We fit the model given by Equation 35 to the shift of the structure function shown in Figure 7 to find the index  $\alpha_1$ . The fit yielded  $\alpha_1 = 1.73$ . The normalized spatial correlation function of flux fluctuations for the space-ground baseline  $\vec{b}_s$  is (Equation 20) :  $|B_u(\vec{b}_s)|^2 = 0.20$ .

From the projected length of the ground-space baseline  $b_s = 6 \times 10^9$  cm we find  $b_{dif}$ :

$$b_{dif} = \frac{z}{(z-z_1)} \frac{1}{k\theta_{scat,1}} = 4.6 \times 10^9 \text{ cm} \quad (40)$$

Using the measured proper motion of  $\mu_\alpha = 17 \pm 4$  mas yr<sup>-1</sup>,  $\mu_\delta = 32 \pm 6$  mas yr<sup>-1</sup> ([Zou et al. 2005](#)), and an assumed distance to the pulsar  $z = 1$  kpc ([Cordes & Lazio 2003](#)), we obtain a pulsar tangential velocity of  $\vec{V}_p = 200$  km/s. Comparison of  $|\vec{V}_p| \Delta t_{dif}$  with  $b_{dif}$  yields  $z_1/(z-z_1) = b_{dif}/|\vec{V}_p| = 0.78$ . Hence,  $z_1 = 0.44 z = 440$  pc. Therefore, the screen is located approximately halfway between the pulsar and the observer. From knowledge of  $b_{dif}$  and  $z_1$ , we obtain  $\theta_{scat,1} = 1.2$  mas. In the observer plane,  $\theta_{obs,1} = [(z-z_1)/z] \theta_{scat,1} = 0.7$  mas.

The normalized frequency correlation function  $R(\Delta f)$  of intensity variations is determined by the diffractive scintillations. [Ostshov & Shishov \(1977\)](#) found that  $R(\Delta f)$  is:

$$R(\Delta f) = 1 - \frac{1}{2} \left( \frac{\Delta f}{\Delta f_{dif}} \right)^{\alpha_1/2}, \quad \Delta f < 2\Delta f_{dif} \quad (41)$$

$$\Delta f_{dif} = \frac{c}{4\pi A(\alpha_1) z (z_1/(z-z_1)) (\theta_{obs,1})^2}$$

Taking  $\alpha_1 = 1.73$ , we find for the constant  $A$ :

$$A(\alpha_1) = [2\Gamma(1 + \alpha_1/2) \cos(\pi\alpha_1/4)]^{\frac{2}{\alpha_1}} \approx 0.34 \quad (42)$$

where  $\Gamma$  is the complete gamma function. Using our estimated values for  $z_1$  and  $\theta_{scat,1}$ , we find  $\Delta f_{dif} = 290$  kHz, which coincides very well with our measured value of  $\Delta f_{dif} = 330$  kHz.

If we suppose the scattering material is homogeneously

distributed between observer and pulsar, then the frequency diffraction scale will be determined by the relations:

$$\Delta f_{dif} = \frac{c}{4\pi B(\alpha_1)z(\theta_{obs,1})^2} \quad (43)$$

$$B(\alpha_1) = \left[ \frac{2(\Gamma(1 + \alpha_1/2))^3 \cos(\pi\alpha_1/4)(1 + \alpha_1)}{\Gamma(2 + \alpha_1)} \right]^{2/\alpha_1} \approx 0.18 \quad (44)$$

We obtain  $\Delta f_{dif} = 430$  kHz, which also coincides with the observations. Thus, our measurement of  $\Delta f_{dif}$  agrees with either a thin-screen model (located at  $z_1 \approx 0.44z$ ) or with homogeneously distributed scattering material, to about the 30% accuracy of our measurement. The consistency of the measured and calculated frequency scales suggests that the assumed pulsar distance of  $z = 1$  kpc corresponds to the actual distance.

The spatial correlation function for weak scintillations from the inhomogeneities of the layer  $z_2$  can be represented as (Smirnova et al. 2014)

$$R(\Delta\vec{\rho}_2) = D_{S,2}(\Delta\rho_{2,Fr}) - D_{S,2}(\Delta\vec{\rho}_2) \quad (45)$$

$$= D_{S,2}(\Delta\rho_{2,Fr}) \left[ 1 - \left( \frac{\Delta\rho_2}{\Delta\rho_{2,Fr}} \right)^{\alpha_2} \right],$$

with :  $|\Delta\vec{\rho}_2| \ll \Delta\rho_{2,Fr}$

where:

$$\Delta\rho_{2,Fr} = \sqrt{\frac{z_2}{k}} \quad (46)$$

Here  $\Delta\vec{\rho}_2$  is the separation of points in the observer's plane (and, equivalently, in the near phase screen at distance  $z_2$ ).

The frequency-time correlation function can be obtained by the replacement  $\Delta\vec{\rho}_2 \rightarrow \Delta\vec{\rho}_{2,t} + \Delta\vec{\rho}_{2,f}$ , where

$$\Delta\vec{\rho}_{2,\Delta f} = -2z_2(\Delta f/\nu_0)\vec{\theta}_{ref,0} \quad (47)$$

$$\Delta\vec{\rho}_{2,\Delta t} = \vec{V}_{obs}\Delta t \quad (48)$$

Here  $\vec{V}_{obs}$  is the observer's velocity. Figure 1 shows that the frequency structure of the diffraction pattern drifts in time, with the speed  $df/dt = 1.5$  MHz/1000 s, so that diffraction spots are extended correspondingly in the dynamic spectrum. The component of velocity  $\vec{V}_{obs}$  parallel to the refraction angle  $\vec{\theta}_{ref,0}$  defines this drift. It produces the shift with time lag of the minimum in frequency of the structure function, as shown in Figure 9. The component of velocity perpendicular to  $\vec{\theta}_{ref,0}$  does not contribute to the shift, but does produce an asymmetry of the structure function about the frequency lag of the minimum,  $f_{min}$ . Specifically, the structure function becomes flatter for frequency lags smaller than  $f_{min}$  and steeper for frequency lags more than  $f_{min}$ . It is difficult to distinguish such an asymmetry at large time shifts because of strong influence of noise. However when  $\vec{V}_{obs}$  is parallel to the refraction angle  $\vec{\theta}_{ref,0}$  features in the dynamic spectra are strongly elongated, as we observe. This suggests that the perpendicular component of velocity is small compared with the parallel component, and we conclude that the vectors  $\vec{V}_{obs}$  and  $\vec{\theta}_{ref,0}$  are approximately parallel. In this case, we can represent the frequency-time correlation function as

$$R(\Delta\vec{\rho}_2) = D_{S,2}(\Delta\vec{\rho}_{2,Fr}) \left( 1 - \frac{1}{2} \left[ \frac{t}{t_{2,0}} - \frac{f}{f_{2,0}} \right]^{\alpha_2} \right) \quad (49)$$

From the shift of  $f_{min}$  for the largest time shift of  $\Delta t =$

640  $P_1$  (Figure 9),  $f_{2,0} = 1.1$  MHz, we find  $t_{2,0} = f_{2,0}(df/dt)^{-1} = 700$  s.

The observer's velocity relative to the Local Standard of Rest, perpendicular to the pulsar's line of sight for the date of our observation, was  $\vec{V}_{obs} = 23.7$  km s<sup>-1</sup>. Using this value, we find for the Fresnel scale  $\Delta\rho_{2,Fr} = 2^{1/\alpha_2}V_{obs}t_{2,0} = 2.5 \times 10^9$  cm, using  $\alpha_2 = 1.73$ . The observer velocity is the vector sum of the velocity of orbital motion of the Earth on the date of observation and the velocity of the Sun relative to the Local Standard of Rest projected to perpendicular to the pulsar's line of sight. We do not know the velocity of the clouds of turbulent plasma responsible for scintillation, but we assume they have velocity relative to the observer of  $|\vec{V}_{scr}| \approx 10$  km s<sup>-1</sup> or less, although we do not know its direction and magnitude. The Fresnel scale we find corresponds to  $\vec{V}_{scr} = 0$ . If we assume that the screen has the velocity of 10 km/s the error in evaluation of  $\Delta\rho_{2,Fr}$  will be  $0.75 \times 10^9$  cm (about 30%). Accordingly, the distance to the near layer is  $z_2 = 0.14 \pm 0.05$  pc. Using Equations 47 and 49 with  $\Delta f = f_{2,0}$ , we obtain  $\theta_{ref,0} = 110 \pm 30$  mas.

We found above that the relative amplitude of the second component is 0.15. Hence,

$$D_{S,2}(\Delta\rho_{2,Fr}) = (k\theta_{scat,2}\Delta\rho_{2,Fr})^{\alpha_2} = 0.15 \quad (50)$$

For  $\alpha_2 = 1.73$  we find  $\theta_{scat,2} = 0.4$  mas. The error of  $\theta_{scat,2}$  is about 30%.

From the condition that the cosmic prism has no significant effect on the frequency correlation of diffractive scintillations, we can estimate an upper limit for the distance to the cosmic prism  $z_{prism}$ . Change in the refraction angle of the cosmic prism with change of frequency  $f$  displaces the diffraction pattern from the strongly-scattering far screen. We assume that the frequency scale of the pattern  $\Delta f_{dif}$  is less than the offset of the scattering from refraction. We then obtain the displacement

$$2(\Delta f_{dif}/\nu_0)z_{prism}\theta_{ref,0} < b_{dif} = 4.6 \times 10^9 \text{ cm} \quad (51)$$

Substituting our observed values of  $\Delta f_{dif} = 330$  kHz and  $\theta_{ref,0} = 110$  mas into this inequality, we find  $z_{prism} \leq 1.4$  pc, or  $z_{prism} \leq 2$  pc when we include the error in our estimate of  $\theta_{ref}$ .

Thus, we find 3 components that contribute to scintillation of pulsar B1919+21: distant material at  $z_1 \approx 440$  pc, or material homogeneously distributed along the line of sight to the pulsar; a cosmic prism at a distance  $z \leq 2$  pc, and a nearby screen at  $z_2 = 0.14$  pc. Most pulsars show some scattering distributed along the line of sight, and the distant material indicates that B1919+21 is no exception.

Cosmic prisms are seen for a number of nearby pulsars. Shishov et al. (2003) found the first evidence for such a component, from analysis of multifrequency observations they found a refraction angle in the direction to PSR B0329+54 of about 0.6 mas at frequency 1 GHz. They inferred that the size of irregularities responsible for refraction is less or about  $3 \times 10^{15}$  cm. Smirnova et al. (2006) found an indication that refractive effects dominate scattering for the direction to PSR J0437-4715. Smirnova et al. (2014) found a cosmic prism in the direction of PSR B0950+08 using space-ground interferometry. The refraction angle was measured as 1.1 to 4.4 mas at frequency 324 MHz. Here, we report the first localization of a cosmic prism, at a distance of about 1.4 pc in the direction to PSR

B1919+21. The material associated with this prism is unknown. However, distances of only a few pc are inferred for the material that is responsible for the scintillation of intraday variable extragalactic sources (Kedziora-Chudczer et al. 1997; Dennett-Thorpe & deBruyn 2002; Bignall et al. 2003; Dennett-Thorpe & deBruyn 2003; Jauncey et al. 2003; Bignall et al. 2006). This material may lie at interfaces where nearby molecular clouds collide (Linsky et al. 2008).

The distance that we find for the close screen, of only 0.14 pc, is extremely close. It lies hundreds of times further away than the termination shock of the solar wind, but within the Oort cloud, and hence within our Solar System. Our observation is the first detection of scattering by ionized gas in this region. Clearly, additional observations are needed to clarify the position and distribution of this material, and its relation to other plasma components of the Solar System and the solar neighborhood.

## 6 CONCLUSION

We have successfully conducted space-ground observations of PSR B1919+21 at frequency 324 MHz with a projected space-ground baseline of 60,000 km. Analysis of frequency and time correlation functions and structure functions provides an estimate of the spatial distribution of interstellar plasma along the line of sight. We show that the observations indicate the existence of two components of scattering material in this direction. One is a screen located at a distance of about 440 pc from the observer, or distributed homogeneously along the line of sight. This shows strong diffractive scintillations and produces the largest effect. The second component is in a much closer screen, at a distance of about 0.14 pc, and corresponds to weak scintillation. The Fresnel scale is equal to  $2.5 \times 10^9$  cm at the near screen. Furthermore, a cosmic prism is located beyond the near screen, leading to a drift of the diffraction pattern across the dynamic spectrum at a speed of  $df/dt = 1.5$  MHz/1000 s. We have estimated the refraction angle of this prism as  $\theta_{ref,0} = 110$  mas, and obtained an upper limit for the distance to the prism:  $z_{prism} \leq 2$  pc. Analysis of the spatial coherence function for the space-ground baseline (RA-GB) allowed us to estimate the scattering angle in the observer plane:  $\theta_{scat} = 0.7$  mas. From temporal and frequency structure functions analysis we find for the index of interstellar plasma electron density fluctuations to be  $n = 3.73$ .

## ACKNOWLEDGEMENTS

The RadioAstron project is led by the Astro Space Center of the Lebedev Physical Institute of the Russian Academy of Sciences and the Lavochkin Scientific and Production Association under a contract with the Russian Federal Space Agency, in collaboration with partner organizations in Russia and other countries. We are very grateful to the staff at the Westerbork synthesis array and Green Bank observatory for their support. The study was supported by the program of the Russian Academy of sciences 'Nonsteady and explosive processes in Astrophysics'. C.R.G. acknowledges support of the US National Science Foundation (AST-1008865).

*Facilities:* RadioAstron Space Radio Telescope (Spektr-R), GB, WB.

## REFERENCES

- Andrianov A.S., Girin I.A., Garov V.E., et al. 2014, Vestnik NPO im. S.A. Lavochkina, 3, 55  
 Avdeev V.Yu., Alakoz A.V., Aleksandrov Yu. A., et al. 2012, Vestnik FGUP NPO im. S.A. Lavochkina, 3, 4  
 Bhat, N. D. R., Ord, S. M., Tremblay, S. E., McSweeney, S. J., & Tingay, S. J. 2016, ApJ, 818, 86  
 Bignall, H. E., et al. 2003, ApJ, 585, 653  
 Bignall et al. 2006, ApJ, 262, 1050  
 Cordes J.M, Lazio T.J.W. 2003, Astro-ph 0207156  
 Dennett-Thorpe, J., & de Bruyn, A.G. 2002, Nature 415, 57  
 Dennett-Thorpe, J., & de Bruyn, A.G. 2003, A&A, 404, 113  
 Gwinn C.R. & Johnson M.D. 2011, ApJ, 733, 51  
 Jauncey, D.L., Johnston, H.M., Bignall, H.E., Lovell, J.E.J., Kedziora-Chudczer, L., Tzioumis, A.K., & Macquart, J.-P. 2003, Ap&SS, 288, 63  
 Kardashev N.S., Khartov V.V., Abramov V.V., et al. 2013, ARep, 57, 153  
 Kedziora-Chudczer et al. 1997, ApJ, 490, L9  
 Linsky J.L., Rickett B.J., & Readfield S. 2008, ApJ, 675, 413  
 Ostashov V.E., Shishov V.I. 1977, Radiophysics, 20, 6, 842  
 Prokhorov, A.M., Bunkin, F.V., Gochelashvili, K.S., & Shishov, V.I. 1975 Proc. IEEE, 63, 790  
 Smirnova, T. V.; Shishov, V. I.; Stinebring, D. R. 1998, Astr Rep, 42, 766  
 Shishov V.I., Smirnova, T.V., Sieber, W., Malofeev, V.M., Potapov, V.A., Stinebring, D., Kramer, M., Jessner, A., & Wielebinski, R. 2003, A&A, 404, 557  
 Smirnova, T.V., Gwinn, C.R., Shishov, Vi.I. 2006, A&A, 453, 601  
 Smirnova & Shishov 2008, Astr Rep, 52, 73  
 Smirnova T.V., Shishov V.I., Popov, M. V., Gwinn, C. R., Anderson, J. M., Andrianov, A. S., Bartel, N., Deller, A., Johnson, M. D., Joshi, B. C., Kardashev, N. S., Karuppusamy, R., Kovalev, Y. Y., Kramer, M., Soglasnov, V. A., Zensus, J. A., Zhuravlev V. 2014, ApJ, 786,115  
 Zou W.Z., Hobbs, G., Wang, N., Manchester, R.N., Wu, X.J., & Wang, H.X. 2005, MNRAS, 362, 1189

This paper has been typeset from a  $\text{\TeX}/\text{\LaTeX}$  file prepared by the author.